

Final Draft
of the original manuscript:

Rahman, M.M.; Filiz, V.; Khan, M.M.; Gacal, B.N.; Abetz, V.:
**Functionalization of POSS nanoparticles and fabrication of block
copolymer nanocomposite membranes for CO₂ separation**
In: Reactive and Functional Polymers (2014) Elsevier

DOI: [10.1016/j.reactfunctpolym.2014.07.006](https://doi.org/10.1016/j.reactfunctpolym.2014.07.006)

Functionalization of POSS nanoparticles and fabrication of block copolymer nanocomposite membranes for CO₂ separation

Md. Mushfequr Rahman¹, Volkan Filiz^{1*}, Muntazim Munir Khan¹, Bahadir N. Gacal¹, Volker Abetz^{1,2*}

¹Helmholtz-Zentrum Geesthacht, Institute of Polymer Research, Max-Planck-Straße 1, 21502 Geesthacht, Germany

²University of Hamburg, Institute of Physical Chemistry, Grindelallee 117, 20146 Hamburg, Germany

Corresponding E-mail: volkan.filiz@hzg.de, volker.abetz@hzg.de

Abstract:

Synthesis of methoxy poly(ethylene glycol) (PEG) functionalized polyoctahedral oligomeric silsesquioxanes (POSS) nanoparticles via epoxy ring opening reaction in three different solvents are outlined in this manuscript. The nanoparticles are used as filler for commercial poly(ether-*block*-amide) multiblock copolymer PEBAX[®] MH 1657. The influence of two novel structural features of the synthesized nanofillers on the gas separation performance of nanocomposite membranes are studied on the examples of CO₂/N₂ and CO₂/H₂ gas pairs. These are – i) presence of a dimethylsilyl group as spacer between the cage structure of POSS and the PEG ligand and ii) formation of a tetrahydrofuran (THF) complex. While ideal selectivity characteristics for the matrix polymer are not significantly affected by the presence of fillers, the single gas permeability (determined by time-lag method) is remarkably increased in both cases.

Keywords: Nanocomposite membrane, Epoxide ring opening, PEBAX, POSS.

1. Introduction:

A widespread concern about the deteriorating climate has resulted in a tremendous research effort towards designing process concepts to prevent the emitting CO₂ due to combustion of fossil fuel from reaching the atmosphere. A diverse number of materials and methods are under study for capture, storage and conversion of CO₂ to mitigate the global warming. The emerging and already established concepts for CO₂ capture encounter the challenge of finding an economically feasible and efficient separation technology from effluent gas streams. [1, 2] Low energy requirements and cost effectiveness of membrane gas separation processes have made this technology an ideal candidate in this quest. At present commercial gas separation modules use polymers as membrane material because of the ease of processability. However, polymer membranes possess a tradeoff between permeability and selectivity. In order to achieve the potential of membrane separation technology a control of the membrane material properties on the molecular level is required. [3, 4] Besides chemical modification of the polymer itself, a facile and efficient method towards this attempt is to incorporate nanosized fillers into polymer matrix which is used as selective layer of the membrane. This class of membranes, referred to as polymer nanocomposite membranes or mixed matrix membranes, has recently been extensively explored for gas separation applications. [5-14]

The nanosized fillers can impart desirable structural and functional properties in a polymeric material. The surface functionality of the nanofillers governs the spatial distribution and mediates the interaction with the polymer segments in the direct vicinity of the surface of the nanofillers. Hence, decorating the surface with suitable functionalities is the key to take benefit of the nanosize of the filler and to control the bulk property of the polymer nanocomposite. [15, 16] Polyhedral oligomeric silsesquioxane (POSS) nanostructures, comprised of a hybrid architecture of an inorganic silsesquioxane cage core (diameter 1-3 nm) surrounded by organic functional groups, is often termed as the smallest possible precisely defined silica nanoparticle. The general formula of POSS is (RSiO_{1.5})_n, where n refers to the number of Si atoms in the cage and R is a hydrogen atom or an organic group.[16-19] A variety of POSS containing reactive functionalities which are suitable precursors for grafting or further modification are commercially available. [16, 20] The flexibility to tune the compatibility between the

nanoparticle and the polymer matrix by altering the functional group is quite appealing for the researchers to design polymer composite materials with improved properties by incorporating functionalized POSS nanoparticles. [21] For gas separation applications POSS incorporated nanocomposite membranes prepared by both physical blending [17, 19, 22, 23] and chemical crosslinking [24] have been reported.

The use of block copolymers instead of homopolymers as matrix material for nanocomposite gives rise to added sophistication for tailoring the material architecture. A complex interplay of both enthalpy and entropy dictates the dispersion and location of nanoparticles in microphase separated block copolymer matrices. A balance between the sizes of nanoparticle and block copolymer domain is the key parameter for controlling the entropic interaction. An efficient method of controlling the enthalpy interactions is the modification of the nanoparticle surface by grafting of organic ligands. These should be chemically compatible with one of the blocks of the block copolymer. [25-29] Quite recently we have reported the influence of PEG POSS[®] (poly(ethylene glycol) functionalized POSS) incorporation in two grades of the commercial poly(ether-*block*-amide) thermoplastic elastomer PEBAX[®] upon CO₂ separation performance.[30, 31] From a thorough investigation of the spatial distribution of PEG POSS[®] within the membrane, thermal and gas transport properties of obtained nanocomposite materials we concluded that the PEG ligand of the PEG POSS[®] plasticizes the polyether segments of PEBAX[®] MH 1657 (containing 60 wt% of poly(ethylene oxide) and 40 wt% of polyamide-6) which leads to increased gas permeability through the membrane. On the other hand incompatibility between the PEG ligand of PEG POSS[®] and polyether block of PEBAX[®] 2533 (containing 80wt% of poly(tetramethylene oxide) and 20wt% of polyamide-12) leads to segregated PEG POSS[®] rich domains which hinders the diffusion of CO₂ in the nanocomposite membrane. [30] In this work we extend that concept to PEG functionalized POSS nanoparticles containing an additional functionality in between the PEG ligand and the silsesquioxane cage core as filler for PEBAX[®] MH 1657 membrane. In what follows, first we aim to provide a comprehensive account of the influence of three different solvents (chloroform, toluene and tetrahydrofuran) upon modification of glycidyl POSS[®] (Scheme 1a) and glycidyl dimethylsilyl POSS[®] (Scheme 1b) with methoxy poly(ethylene glycol) (PEG) via epoxide ring opening

reaction. Next we compare the CO₂ separation performance of the nanocomposite membranes fabricated by using the obtained functionalized nanoparticles as filler for PEBAX[®] MH 1657.

Scheme 1

2. Experimental part:

2.1. Materials:

Glycidyl POSS[®] and glycidyl dimethylsilyl POSS[®] are purchased from Hybrid Plastics[®]. PEBAX[®] MH 1657 is purchased from ARKEMA. Methoxy poly(ethylene glycol) (M_n=350 g/mol) is purchased from Sigma-Aldrich. The solvents chloroform, toluene, tetrahydrofuran and ethanol were purchased from Merck KGaA.

2.2. Modification of glycidyl POSS[®] and glycidyl dimethylsilyl POSS[®] with methoxy poly(ethylene glycol):

2.2.1. Procedure of functionalization of nanoparticles:

4g (3 mmol) glycidyl POSS[®] and 30g (86 mmol) methoxy poly(ethylene glycol) (PEG) (M_n=350 g/mol) were dissolved in 200g solvent (chloroform, toluene or tetrahydrofuran). Approximately 400μl of boron trifluoride diethyletherate catalyst were added to the reaction mixture and stirred for 48 hours at room temperature. The solvent was removed from the reaction mixture using a rotary evaporator. The reaction mixture was dissolved in dichloromethane and 100 g 2wt% aqueous solution of NaOH was added to convert the remaining catalyst into salt. The unreacted PEG and the salt were removed from the mixture by dichloromethane and water extraction. Extraction was continued until the entire unreacted PEG fraction was removed (confirmed by ¹³C-NMR spectra). The PEG modified glycidyl POSS was collected in the organic phase. The organic phase was dehydrated using MgSO₄ salt and filtered. Finally, dichloromethane was evaporated to collect the product. Using the same procedure methoxy

poly(ethylene glycol) ($M_n=350$ g/mol) modified glycidyl dimethylsilyl POSS[®] was also synthesized. The resulting products from the synthesis are given acronym in Table 1.

2.2.2. Characterization of the POSS nanoparticles:

FT-IR spectra were recorded on an attenuated total reflectance (ATR-diamond crystal) mode with a Bruker ALPHA FT-IR spectrometer in a spectral range of 400-4000 cm^{-1} with a resolution of 2 cm^{-1} and average of 32 scans. Thermogravimetric analysis (TGA) was done using a Netzsch TG209 F1 Iris instrument under argon flow from 25 °C to 1000 °C at 2K/min. NMR spectroscopic measurements were performed on a Bruker AV300 spectrometer at a sample temperature of 298K using CDCl_3 as solvent. ^1H -NMR spectra were recorded applying a 10ms 90° pulse. ^{13}C -NMR spectra were recorded using DEPTQ-135 sequences employing a waltz-16 decoupling scheme to determine multiplicity. Quantitative ^{13}C -NMR spectra were recorded using an inverse gated decoupled sequence. The lists of peaks of all the NMR spectra are provided below.

a) PEG-GLY-POSS-Chloroform

^1H NMR (CDCl_3 , 300 MHz): δ (ppm): 0.61(s, 2H), 1.21 (t, 3H), 1.65 (s, 2H), 3.38 (s, 3H), 3.4-4.0 (m, $-\text{CH}_2\text{CH}_2\text{O}-$ of PEG).

$^{13}\text{C}\{^1\text{H}\}$ NMR (CDCl_3 , 75 MHz): δ (ppm): 8.6, 15.1, 23.0, 59.0, 66.7, 69.3, 70.5, 71.9, 72.7, 73.5.

b) PEG-GLY-POSS-Toluene

^1H NMR (CDCl_3 , 300 MHz): δ (ppm): 0.62 (s, 2H), 1.65 (s, 2H), 3.38 (s, 3H), 3.4-4.0 (m, $-\text{CH}_2\text{CH}_2\text{O}-$ of PEG).

$^{13}\text{C}\{^1\text{H}\}$ NMR (CDCl_3 , 75 MHz): δ (ppm): 8.6, 23.0, 59.0, 69.4, 70.5, 71.9, 72.7, 73.5.

c) PEG-GLY-POSS-THF

^1H NMR (CDCl_3 , 300 MHz): δ (ppm): 0.61(s, 2H), 1.62 (s, overlapped $-\text{CH}_2$ of THF and $-\text{CH}_2$ of glycidyl arm), 3.38 (s, 3H), 3.4-4.0 (m, overlapped $-\text{CH}_2$ of THF & $-\text{CH}_2\text{CH}_2\text{O}-$ of PEG).

$^{13}\text{C}\{^1\text{H}\}$ NMR (CDCl_3 , 75 MHz): δ (ppm): 8.6, 23.0, 26.5, 59.0, 69.4, 70.0, 70.5, 71.1, 71.3, 71.9, 73.6.

d) PEG-GDMS-POSS-Chloroform

^1H NMR (CDCl_3 , 300 MHz): δ (ppm): 0.14, (s, 6H), 0.58 (s, 2H), 1.21 (t, 3H), 1.61 (s, 2H), 3.38 (s, 3H), 3.4-4.0 (m, $-\text{CH}_2\text{CH}_2\text{O}-$ of PEG).

$^{13}\text{C}\{^1\text{H}\}$ NMR (CDCl_3 , 75 MHz): δ (ppm): -0.4, 13.6, 15.1, 23.0, 59.0, 66.7, 69.3, 70.5, 71.9, 72.7, 74.1.

e) PEG-GDMS-POSS-Toluene

^1H NMR (CDCl_3 , 300 MHz): δ (ppm): 0.14, (s, 6H), 0.58 (s, 2H), 1.61 (s, 2H), 3.38 (s, 3H), 3.4-4.0 (m, $-\text{CH}_2\text{CH}_2\text{O}-$ of PEG).

$^{13}\text{C}\{^1\text{H}\}$ NMR (CDCl_3 , 75 MHz): δ (ppm): -0.4, 13.6, 23.0, 59.0, 69.3, 70.5, 71.9, 72.7, 74.1.

f) PEG-GDMS-POSS-THF

^1H NMR (CDCl_3 , 300 MHz): δ (ppm): 0.14, (s, 6H), 0.61(s, 2H), 1.62 (s, overlapped $-\text{CH}_2$ of THF and $-\text{CH}_2$ of glycidyl arm), 3.38 (s, 3H), 3.4-4.0 (m, overlapped $-\text{CH}_2$ THF & $-\text{CH}_2\text{CH}_2\text{O}-$ of PEG).

$^{13}\text{C}\{^1\text{H}\}$ NMR (CDCl_3 , 75 MHz): δ (ppm): -0.4, 13.6, 23.1, 26.5, 59.0, 69.4, 70.0, 70.5, 71.1, 71.3, 71.9, 74.1.

2.3. Preparation and characterization of the nanocomposite membranes:

Nanocomposite membranes containing the synthesized PEG modified POSS as nanofillers and the PEBAX® MH 1657 as matrix were prepared via solution casting method. The nanofiller content was varied from 10 - 40 wt% in respect to the resulting nanocomposite. 3 wt% solution of mixture of polymer and filler were prepared in a mixture of ethanol/water (70/30 wt %) under reflux (80 °C) for 2h. The obtained homogeneous solution was cooled down to room temperature and poured into Teflon molds. Nanocomposite membranes were obtained by drying the solution at 40°C for 24 hours. The thickness of the membranes was measured by a digital micrometer which is in the range of 100 – 200 µm.

The nanocomposite membranes were characterized via constant volume, variable pressure (“time-lag”) method. Single gas permeability of N₂, H₂ & CO₂ were determined within the temperature range 30 °C to 70 °C. The feed pressure was set to 1 bar for all the gases. The following equations were used to determine gas permeability (P), diffusion coefficient (D), solubility (S) and ideal selectivity for pure gases ($\alpha_{A/B}$), respectively –

$$P = D \cdot S = \frac{V_p \cdot l}{A \cdot R \cdot T \cdot \Delta t} \ln \frac{p_f - p_{p1}}{p_f - p_{p2}} \quad (1)$$

$$D = \frac{l^2}{6\theta} \quad (2)$$

$$\alpha_{A/B} = \frac{P_A}{P_B} \quad (3)$$

where, V_p is the permeate volume, l is the membrane thickness, A is the membrane area, R is the gas constant, p_f is the feed pressure considered constant in the time range Δt , p_{p1} and p_{p2} are

permeate pressures at the times 1 and 2, respectively, and Δt is the time difference between these two points (1 and 2) on the pressure curve, and θ is the time lag.

3. Results and discussion:

3.1. Modification of glycidyl POSS[®] and glycidyl dimethylsilyl POSS[®] with methoxy poly(ethylene glycol):

Scheme 2

Epoxides (three membered oxiranes) are extremely strained and reactive systems. Scheme 2 illustrates the two possible routes of an asymmetric epoxide ring opening reaction. One is following the S_N1 mechanism (Scheme 2, Route A) where nucleophilic substitution occurs at the more substituted carbon. In this reaction pathway the breaking of C-O bond creates a carbocation and the nucleophile attacks this carbocation. Hence, the stability of the carbocation determines the nucleophilic attack at this position to a great extent. The other possibility is that the reaction follows the S_N2 mechanism (Scheme 2, Route B) where the nucleophile attacks the less substituted carbon. The driving force of this reaction pathway is provided more by electron transfer from carbon to oxygen than by electron transfer from the nucleophile to the carbon. Under acidic conditions the position of attack of the nucleophile is determined both by the steric hindrance and the carbocation stability. [32]

Figure 1

To justify the epoxide ring opening and subsequent attachment of PEG ligand, the synthesis was monitored by NMR and FT-IR spectroscopy. Figure 1b and Figure 2 illustrates the ¹³C-DEPTQ-135 NMR and FT-IR spectra of glycidyl POSS[®] (i), PEG (ii) and PEG functionalized glycidyl POSS using toluene as solvent (iii). In the ¹³C DEPTQ-135 NMR spectra of Figure 1b the –CH

and $-\text{CH}_3$ peaks are pointed upwards and the $-\text{CH}_2$ peaks are pointed downwards. The peaks E and F at 44.3 ppm and 50.9 ppm, respectively, in spectrum (i) originate from the epoxide ring of glycidyl POSS[®] and the peak P at 61.6 ppm in spectrum (ii) is attributed to the neighboring $-\text{CH}_2$ of $-\text{OH}$ group of PEG. Disappearance of the peaks E, F & P in spectrum (iii) and strong appearance of the peaks Y', U' and V' at 59 ppm and 70.5 ppm which originates from $-\text{CH}_3$ end group and $-\text{CH}_2\text{-O-CH}_2\text{-}$ repeating unit of PEG, respectively, proves the successful modification of glycidyl POSS[®] with PEG. Spectrum (iii) shows only one $-\text{CH}$ peak at 69.3 ppm (peak E'). Hence, the reaction followed one particular route of Scheme 2 (either $\text{S}_{\text{N}}1$ or $\text{S}_{\text{N}}2$ mechanism). The position of the peak E' suggests that in the present case the epoxide ring opening occurred via route B i.e $\text{S}_{\text{N}}2$ mechanism. Because in the other case, ($\text{S}_{\text{N}}1$ mechanism) the $-\text{CH}$ peak is expected to appear more downfield.

Figure 2

In the FT-IR spectrum of glycidyl POSS[®] (Figure 2, spectrum (i)) the Si–O–Si stretching vibration of POSS cage and the C–O–C stretching vibration of epoxide group are detected at 1090 cm^{-1} and 907 cm^{-1} , respectively.[33] The stretching vibration of $-\text{OH}$ group, C–H stretching vibration of the methylene group and C–O stretching vibration of the $-\text{CH}_2\text{-O-CH}_2\text{-}$ repeating unit of PEG are observed at 3467 cm^{-1} , 2866 cm^{-1} and 1096 cm^{-1} , respectively, (Figure 2, spectrum (ii)). In the FT-IR spectrum of the PEG modified glycidyl POSS (Figure 2, spectrum (iii)) Si–O–Si stretching vibration of POSS and C–O stretching vibration of the $-\text{CH}_2\text{-O-CH}_2\text{-}$ repeating unit of PEG overlap each other and the presence of $-\text{OH}$ group is evident from the band at 3455 cm^{-1} . Since the peak P (the neighboring $-\text{CH}_2$ peak of $-\text{OH}$ group of PEG) completely disappeared in the NMR spectra (Figure 1, spectrum (iii)) there is no unreacted PEG left. A new $-\text{OH}$ group originates after epoxy ring opening which gives the broad peak at 3455 cm^{-1} in FT-IR (Figure 2, spectrum (iii)). The combination of ^{13}C -NMR and FT-IR results leads to the conclusion of structure (iii) of Figure 1.

3.2. Influence of solvent upon the structure of functionalized POSS nanoparticles:

Both glycidyl POSS[®] and glycidyl dimethylsilyl POSS[®] are successfully modified with PEG using three different solvents (chloroform, toluene and THF). For further discussion in this manuscript the product of these reactions are given acronyms (listed in table 1).

Table 1

Figure 3

¹H-NMR and the ¹³C-DEPTQ-135 NMR spectra of the synthesized nanofillers are provided as supplementary information. From the position of the –CH peak after ring opening it is evident that the epoxide ring opening reaction occurred via S_N2 mechanism in all three solvents for both glycidyl POSS[®] and glycidyl dimethylsilyl POSS[®]. The quantitative ¹³C (inverse gated decoupled) NMR spectra of the synthesized nanofillers are presented in Figure 3. Comparison of these spectra as well as the integration of the area of peaks reveals very important information about the structure of the synthesized nanoparticles. If all the epoxide rings open up due to nucleophilic attack of the –OH group of PEG, the integration of the area of –CH₂ peak at 23 ppm and –CH₃ peak (originates from the end group of PEG) at 59 ppm should be equal (since it is already evident that there is no unreacted PEG left in the product). In the spectra of both PEG-GLY-POSS-Toluene (Figure 3b) and PEG-GDMS-POSS-Toluene (Figure 3e) the integral areas of these peaks are nearly equal. Hence, it is clear that toluene as a solvent for the reaction does not lead to any byproducts and the epoxide ring opening occurs merely due to nucleophilic attack of PEG. However, in the spectra of PEG-GLY-POSS-Chloroform (Figure 3a) and PEG-GDMS-POSS-Chloroform (Figure 3d) two additional peaks are visible at 66.7 ppm and 15.1 ppm. These peaks are a distinct signature of the –OCH₂CH₃ group of boron trifluoride diethyletherate i.e. the catalyst. Moreover, the integral areas of –CH₃ peak at 59 ppm with respect to the areas of –CH₂ peak at 23 ppm are not equal. These observations unveil the fact that when chloroform is used as the reaction solvent, although most of the epoxide rings (ca. 80%) are opened by the PEG, a small fraction of epoxide rings are opened by the catalyst itself. Comparison of the integral area of the –CH₂ peak at 70.5 ppm (originating from the repeating unit of PEG) of Figures 3a to 3d

and Figures 3b to 3e also supports this argument and provides evidence that PEG-GLY-POSS-Chloroform (Figure 3a) and PEG-GDMS-POSS-Chloroform (Figure 3d) contains less amount of PEG compared to PEG-GLY-POSS-Toluene (Figure 3b) and PEG-GDMS-POSS-Toluene (Figure 3e), respectively. However, there is some deviation in the integral areas of this peak due to closely packed peaks (baseline is difficult to be determined) at this region. In the NMR spectra of PEG-GLY-POSS-THF (Figure 3c) and PEG-GDMS-POSS-THF (Figure 3f), although no peak is observed which may originate from the catalyst, a typical peak for THF is observed at 26.5 ppm and another peak is merged with the repeating unit of PEG at 70.5 ppm. Two individual resonances for protons of the THF are clearly visible in the $^1\text{H-NMR}$ spectra at 1.62 ppm and 3.41 ppm (spectra provided in supplementary information). Moreover, in $^{13}\text{C-NMR}$ of PEG-GLY-POSS-THF (Figure 3c) and PEG-GDMS-POSS-THF (Figure 3f) three new peaks are observed at 70 ppm, 71.1 ppm and 71.3 ppm. But the areas of $-\text{CH}_2$ peak at 23 ppm and $-\text{CH}_3$ at 59 ppm are rather similar. Hence it can be concluded that the epoxide rings are opened by a nucleophilic attack of PEG.

Figure 4

Figure 5

Thermogravimetric analysis (TGA) of glycidyl POSS[®] and glycidyl dimethylsilyl POSS[®] before and after PEG modification are presented in Figures 4 and 5, respectively. The weight loss of PEG starts at 221 °C and there is no significant residue at the end. It is evident that the thermal stability of the PEG ligand attached to POSS is higher compared to that of pure PEG. For glycidyl POSS[®] (Figure 4) and glycidyl dimethylsilyl POSS[®] (Figure 5) the onset temperature of mass loss are 337 °C and 327 °C while the residual masses are 44.1% and 38.1%, respectively. After grafting PEG to the POSS nanoparticles the mass loss increases substantially which is attributed to the higher organic functional group content of the POSS. No significant difference is observed in the residual mass of PEG-GLY-POSS-Chloroform, PEG-GLY-POSS-Toluene, PEG-GDMS-POSS-Chloroform and PEG-GDMS-POSS-Toluene. But, both PEG-GLY-POSS-THF (Figure 4) and PEG-GDMS-POSS-THF (Figure 5) show higher mass loss compared to the

POSS nanoparticles modified using chloroform and toluene as solvent. The onset of mass loss for PEG-GLY-POSS-THF (Figure 4) and PEG-GDMS-POSS-THF (Figure 5) are 314 °C and 310 °C, respectively. Hence the higher mass loss is not due to the presence of any residual solvent. It must be attributed to an organic moiety which is strongly bound to the POSS nanoparticles. The observations of ^{13}C -NMR and TGA leads to a conjecture that THF forms a complex when it is used as solvent for epoxide ring opening reaction in presence of boron trifluoride diethyletherate catalyst i.e. in PEG-GLY-POSS-THF and PEG-GDMS-POSS-THF.

3.3. Gas separation performance of the nanocomposite membranes:

In this section, the gas separation performance of the prepared nanocomposite membranes is compared with that of the pure PEBA^X® MH 1657 membrane. The solution-diffusion mechanism is adopted to explain the transport of CO₂ gas through the prepared dense membranes.

Figure 6

Figure 6 shows the permeability of N₂, H₂ and CO₂ as a function of nanofiller content in the nanocomposite membranes at 30 °C. By comparing the graphs on the left column of Figure 6 to those on the right column (i.e Figure 6a to 6d, 6b to 6e and 6c to 6f, respectively) it is possible to study the effect of the dimethylsilyl spacer between the cage structure of POSS and PEG ligand on the gas permeability of the nanocomposite membranes. On the other hand, comparison of the graphs of one column with each other (e.g. Figure 6a, 6b and 6c) shows the effect of the three different solvent used for synthesis of the nanofillers upon gas permeability of the nanocomposite membranes. The scale of the graphs in Figures 6 and 7 are similar for easier comparison. It is evident from Figure 6 that the nanocomposite membranes containing the nanofillers with the dimethylsilyl spacer i.e. PEG-GDMS-POSS-Chloroform (Figure 6d), PEG-GDMS-POSS-Toluene (Figure 6e) and PEG-GDMS-POSS-THF (Figure 6f) have higher permeabilities compared to those containing the nanoparticles without spacer i.e. PEG-GLY-

POSS-Chloroform (Figure 6a), PEG-GLY-POSS-Toluene (Figure 6b) and PEG-GLY-POSS-THF (Figure 6c). Comparison of Figure 6a to Figure 6b shows that incorporation of PEG-GLY-POSS-Chloroform and PEG-GLY-POSS-Toluene in PEBAX[®] MH 1657 leads to similar values of gas permeability for all four compositions. Figures 6d and 6e (i.e gas permeability of nanocomposites containing PEG-GDMS-POSS-Chloroform and PEG-GDMS-POSS-Toluene respectively) are also analogous. Therefore, it is clear that although the synthesis of nanofillers in chloroform induces small amounts of byproduct due to ring opening via catalyst instead of PEG, it does not have any significant influence upon gas permeability of the nanocomposite membranes. But Figure 6c shows that the PEG-GLY-POSS-THF incorporated nanocomposites have higher gas permeability compared to the nanocomposites containing both PEG-GLY-POSS-Chloroform (Figure 6a) and PEG-GLY-POSS-Toluene (Figure 6b). Figure 6f shows that the nanocomposites containing up to 30wt% PEG-GDMS-POSS-THF have higher permeabilities compared to the nanocomposites containing PEG-GDMS-POSS-Chloroform (Figure 6d) and the nanocomposites containing PEG-GDMS-POSS-Toluene (Figure 6e) of similar composition.

According to the solution diffusion model the gas permeability through non porous polymer membrane is a product of the kinetic factor diffusion coefficient and the thermodynamic factor solubility. [34] The diffusion and solubility coefficients of CO₂ were determined using equation 2 and 1, respectively. (Supplementary information S 4) All the nanocomposite membranes show higher CO₂ diffusion coefficient compared to PEBAX[®] MH 1657. This phenomenon stems from the fact that the PEG modified POSS nanoparticles act as plasticizer for the polyether blocks of PEBAX[®] MH 1657. Eventually the mobility of the polyether segments of PEBAX[®] MH 1657 increases after incorporation of the nanoparticles which aids faster diffusion of CO₂ through the nanocomposite membranes. Moreover, it is clear that the presence of the THF complex and the dimethylsilyl spacer between the cage structure of POSS and PEG ligand both leads to higher CO₂ diffusion coefficient through the nanocomposite membranes which in turn increases the CO₂ permeability. Therefore, the nanofillers containing the THF complex and the dimethylsilyl spacer increase the mobility of the polyether segment more than the nanofillers which do not have such moiety. The correlation between gas transport mechanism and structure of the nanofillers are discussed in detail elsewhere.[35]

Figure 7

Figure 7 shows the selectivity of CO₂ over N₂ and H₂ as a function of nanofiller content in the nanocomposite membranes at 30°C. The CO₂/N₂ selectivity is unchanged in PEG-GLY-POSS-Chloroform and PEG-GLY-POSS-Toluene containing nanocomposite membranes. However, the nanocomposite membranes containing other fillers show a decreasing trend of CO₂/N₂ selectivity with increasing nanofiller content. The CO₂/N₂ selectivity of PEBAX[®] MH 1657 membrane is 53. At 40 wt% loading of PEG-GLY-POSS-Chloroform, PEG-GLY-POSS-Toluene, PEG-GLY-POSS-THF, PEG-GDMS-POSS-Chloroform, PEG-GDMS-POSS-Toluene & PEG-GDMS-POSS-THF the CO₂/N₂ selectivity of the nanocomposite membranes were 53, 52, 48, 45, 46 and 44, respectively. Hence, presence of the THF complex and the dimethylsilyl spacer between the cage structure of POSS and PEG ligand both leads to marginal loss of CO₂/N₂ selectivity at 30°C. However, it is observed that the CO₂/H₂ selectivity did not change at all in the nanocomposite membranes at 30°C.

From an application point of view, an increase in permeability of the membrane material leads to a decrease of capital investment because less membrane area is required to separate a particular amount of gas. Due to the enormous scale of the gas separation plants even small improvement of permeability of the membrane material can lead to large economic advantage. The investigation of gas separation performance presented in Figure 6 and 7 shows that compared to the nanocomposite containing PEG-GLY-POSS-Chloroform and PEG-GLY-POSS-Toluene those containing PEG-GLY-POSS-THF, PEG-GDMS-POSS-Chloroform, PEG-GDMS-POSS-Toluene and PEG-GDMS-POSS-THF have remarkably higher CO₂ permeability without substantial loss of CO₂/N₂ and CO₂/H₂ selectivity at 30 °C. Hence, the structural features of the PEG functionalized POSS nanoparticle introduced in this paper i.e. the dimethylsilyl spacer and the THF complex are certainly apt to improve the separation efficiency of PEBAX[®] MH 1657 CO₂ selective membrane.

4. Conclusion:

The grafting of PEG ligand to epoxide containing POSS nanoparticles in presence of boron trifluoride diethyletherate catalyst using chloroform, toluene or THF as solvents is thoroughly investigated. Although the epoxide ring opening occurs merely via S_N2 mechanism in all three investigated solvents for both glycidyl POSS[®] and glycidyl dimethylsilyl POSS[®], the choice of solvent has a substantial effect upon the final product obtained from the synthesis. The reaction in toluene occurred without formation of any byproducts, but in chloroform a small fraction of the epoxide rings are opened by the catalyst itself. When THF was used as solvent for the reaction, the solvent molecules formed a complex (in PEG-GLY-POSS-THF and PEG-GDMS-POSS-THF). While the collective information from NMR and TGA indicates formation of the THF complex, the exact nature of this complex remains unclear.

The intriguing structural features of the synthesized nanoparticles have eventually led us to design some innovative block copolymer nanocomposite membranes for CO₂ separation based on the commercial thermoplastic elastomer PEBAX[®] MH 1657. The single gas permeability results of the nanocomposites containing 10-40 wt% of the synthesized nanofillers confirm that the dimethylsilyl spacer between the cage structure of POSS and the PEG ligand enhanced the gas permeability through the nanocomposite membranes. The THF complex (in PEG-GLY-POSS-THF and PEG-GDMS-POSS-THF) also increased the gas permeability of the nanocomposite membranes. Moreover, no substantial loss of CO₂/N₂ selectivity and CO₂/H₂ selectivity was observed. In short, this paper demonstrates that incorporation of the PEG functionalized POSS nanoparticles containing dimethylsilyl spacer and THF complex are very promising to improve the CO₂ separation performance of PEBAX[®] MH 1657 from N₂ and H₂. Therefore, it is essential to precisely control these structural features of the nanoparticles to design new generation of polymer nanocomposite membranes with controlled molecular functions.

Acknowledgment:

The authors gratefully acknowledge Sergey Shishatskiy for helpful discussion on gas separation performance of the membranes. Mona Wambach, Thomas Emmeler and Silvio Neumann are also acknowledged for their suggestion and technical support in NMR study. This work was financially supported by the Helmholtz Association of German Research Centres through the Helmholtz Portfolio MEM-BRAIN.

References:

- [1] D.M. D'Alessandro, B. Smit, J.R. Long, *Angewandte Chemie International Edition*, 49 (2010) 6058-6082.
- [2] M. Ashley, C. Magiera, P. Ramidi, G. Blackburn, T.G. Scott, R. Gupta, K. Wilson, A. Ghosh, A. Biswas, *Greenhouse Gases: Science and Technology*, 2 (2012) 419-444.
- [3] P. Bernardo, E. Drioli, G. Golemme, *Industrial & Engineering Chemistry Research*, 48 (2009) 4638-4663.
- [4] D.L. Gin, R.D. Noble, *Science*, 332 (2011) 674-676.
- [5] T.C. Merkel, B.D. Freeman, R.J. Spontak, Z. He, I. Pinnau, P. Meakin, A.J. Hill, *Science*, 296 (2002) 519-522.
- [6] Y. Kong, H. Du, J. Yang, D. Shi, Y. Wang, Y. Zhang, W. Xin, *Desalination*, 146 (2002) 49-55.
- [7] N.P. Patel, J.M. Zielinski, J. Samseth, R.J. Spontak, *Macromolecular Chemistry and Physics*, 205 (2004) 2409-2419.
- [8] M. Sadeghi, M.A. Semsarzadeh, H. Moadel, *Journal of Membrane Science*, 331 (2009) 21-30.
- [9] N.P. Patel, A.C. Miller, R.J. Spontak, *Advanced Materials*, 15 (2003) 729-733.
- [10] M.M. Khan, V. Filiz, G. Bengtson, S. Shishatskiy, M.M. Rahman, J. Lillepaerg, V. Abetz, *Journal of Membrane Science*, 436 (2013) 109-120.
- [11] M.M. Khan, V. Filiz, G. Bengtson, S. Shishatskiy, M. Rahman, V. Abetz, *Nanoscale Research Letters*, 7 (2012) 504.
- [12] J. Ahn, W.-J. Chung, I. Pinnau, M.D. Guiver, *J. Membr. Sci.*, 314 (2008) 123-133.
- [13] T.C. Merkel, Z. He, I. Pinnau, *Macromolecules*, 36 (2003) 6844-6855.
- [14] H. Cong, J. Zhang, M. Radosz, Y. Shen, *Journal of Membrane Science*, 294 (2007) 178-185.
- [15] A.C. Balazs, T. Emrick, T.P. Russell, *Science*, 314 (2006) 1107-1110.
- [16] E. Ayandele, B. Sarkar, P. Alexandridis, *Nanomaterials*, 2 (2012) 445-475.
- [17] N. Hao, M. Böhning, A. Schönhals, *Macromolecules*, 43 (2010) 9417-9425.
- [18] L. Chen, B. Zeng, J. Xie, S. Yu, C. Yuan, Y. Pan, W. Luo, X. Liu, K. He, Y. Xu, L. Dai, *Reactive and Functional Polymers*, 73 (2013) 1022-1029.
- [19] K. Madhavan, B.S.R. Reddy, *Journal of Membrane Science*, 342 (2009) 291-299.
- [20] G. Li, L. Wang, H. Ni, C. Pittman, Jr., *Journal of Inorganic and Organometallic Polymers*, 11 (2001) 123-154.
- [21] A. Fina, D. Tabuani, A. Frache, G. Camino, *Polymer*, 46 (2005) 7855-7866.

- [22] P. Iyer, G. Iyer, M. Coleman, *Journal of Membrane Science*, 358 (2010) 26-32.
- [23] H. Ríos-Dominguez, F.A. Ruiz-Treviño, R. Contreras-Reyes, A. González-Montiel, *Journal of Membrane Science*, 271 (2006) 94-100.
- [24] M.L. Chua, L. Shao, B.T. Low, Y. Xiao, T.-S. Chung, *Journal of Membrane Science*, 385–386 (2011) 40-48.
- [25] A.C. Balazs, *Nat Mater*, 6 (2007) 94-95.
- [26] M.R. Bockstaller, R.A. Mickiewicz, E.L. Thomas, *Advanced Materials*, 17 (2005) 1331-1349.
- [27] B. Sarkar, P. Alexandridis, *Langmuir*, 28 (2012) 15975-15986.
- [28] R. Mezzenga, J. Ruokolainen, *Nat Mater*, 8 (2009) 926-928.
- [29] B. Sarkar, E. Ayandele, V. Venugopal, P. Alexandridis, *Macromolecular Chemistry and Physics*, 214 (2013) 2716-2724.
- [30] M.M. Rahman, V. Filiz, S. Shishatskiy, C. Abetz, S. Neumann, S. Bolmer, M.M. Khan, V. Abetz, *Journal of Membrane Science*, 437 (2013) 286-297.
- [31] M.M. Rahman, V. Filiz, S. Shishatskiy, S. Neumann, M.M. Khan, V. Abetz, *Procedia Engineering*, 44 (2012) 1523-1526.
- [32] R.C.D. Muniz Filho, S.A.A.d. Sousa, F.v.d.S. Pereira, M.r.M.C. Ferreira, *The Journal of Physical Chemistry A*, 114 (2010) 5187-5194.
- [33] J. Mu, S. Zheng, *Journal of Colloid and Interface Science*, 307 (2007) 377-385.
- [34] K. Ghosal, B.D. Freeman, *Polymers for Advanced Technologies*, 5 (1994) 673-697.
- [35] M.M. Rahman, S. Shishatskiy, C. Abetz, P. Georgopoulos, M.M. Khan, V. Filiz, V. Abetz, *Journal of Membrane Science*, Accepted.

Scheme captions:

Scheme 1: Structure of (a) glycidyl POSS[®] (b) glycidyl dimethylsilyl POSS[®].

Scheme 2: Two routes of epoxide ring opening reaction mechanism S_N1 and S_N2.

Figure captions:

Figure 1: (a) Reaction scheme and chemical structures (b) ^{13}C -DEPTQ-135 NMR spectra of (i) glycidyl POSS[®] (ii) methoxy poly(ethylene glycol) (PEG) (iii) PEG modified glycidyl POSS.

Figure 2: FT-IR spectra of (i) glycidyl POSS[®] (ii) methoxy poly(ethylene glycol) (PEG) (iii) PEG modified glycidyl POSS.

Figure 3: Quantitative ^{13}C (inverse gated decoupled) NMR spectra of – (a) PEG-GLY-POSS-Chloroform (b) PEG-GLY-POSS-Toluene (c) PEG-GLY-POSS-THF (d) PEG-GDMS-POSS-Chloroform (e) PEG-GDMS-POSS-Toluene (f) PEG-GDMS-POSS-THF.

Figure 4: Thermogravimetric analysis of i) glycidyl POSS[®] ii) PEG-GLY-POSS-Toluene iii) PEG-GLY-POSS-Chloroform iv) PEG-GLY-POSS-THF v) Methoxy PEG.

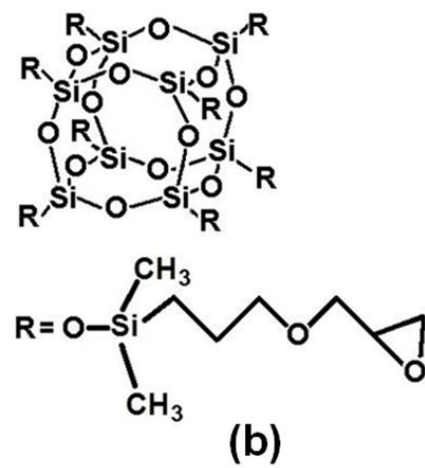
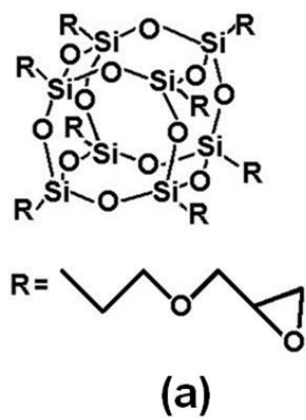
Figure 5: Thermogravimetric analysis of i) glycidyldimethylsilyl POSS[®] ii) PEG-GDMS-POSS-Toluene iii) PEG-GDMS-POSS-Chloroform iv) PEG-GDMS-POSS-THF v) Methoxy PEG.

Figure 6: Single gas permeability as a function of- a) PEG-GLY-POSS-Chloroform content b) PEG-GLY-POSS-Toluene content c) PEG-GLY-POSS-THF content d) PEG-GDMS-POSS-Chloroform content e) PEG-GDMS-POSS-Toluene content f) PEG-GDMS-POSS-THF content. Permeability of N_2 and H_2 are plotted on left Y axis and that of CO_2 right Y axis.

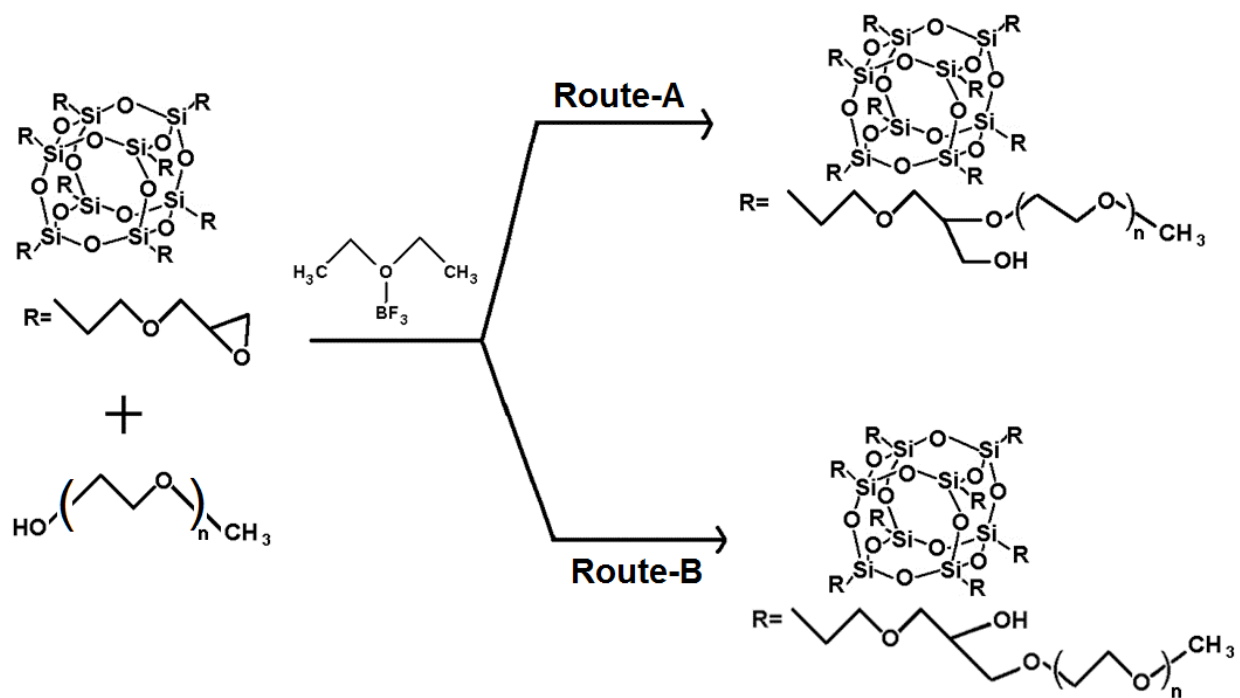
Figure 7: CO_2 selectivity over light gases as a function of: a) PEG-GLY-POSS-Chloroform content b) PEG-GLY-POSS-Toluene content c) PEG-GLY-POSS-THF content d) PEG-GDMS-POSS-Chloroform content e) PEG-GDMS-POSS-Toluene content f) PEG-GDMS-POSS-THF content.

Table caption:

Table 1. Acronyms of the products of epoxide ring opening reaction.



Scheme 1



Scheme 2

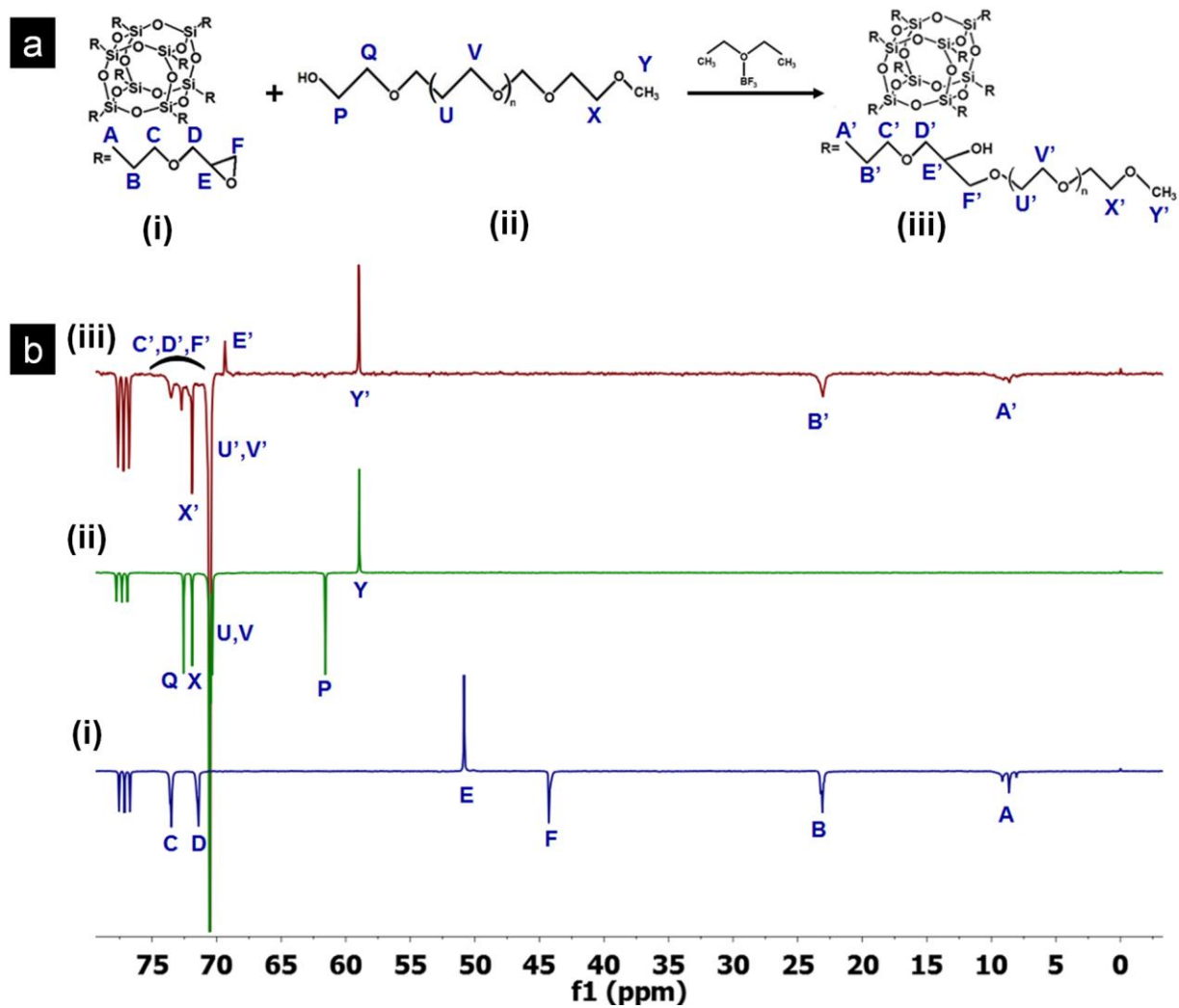


Figure 1

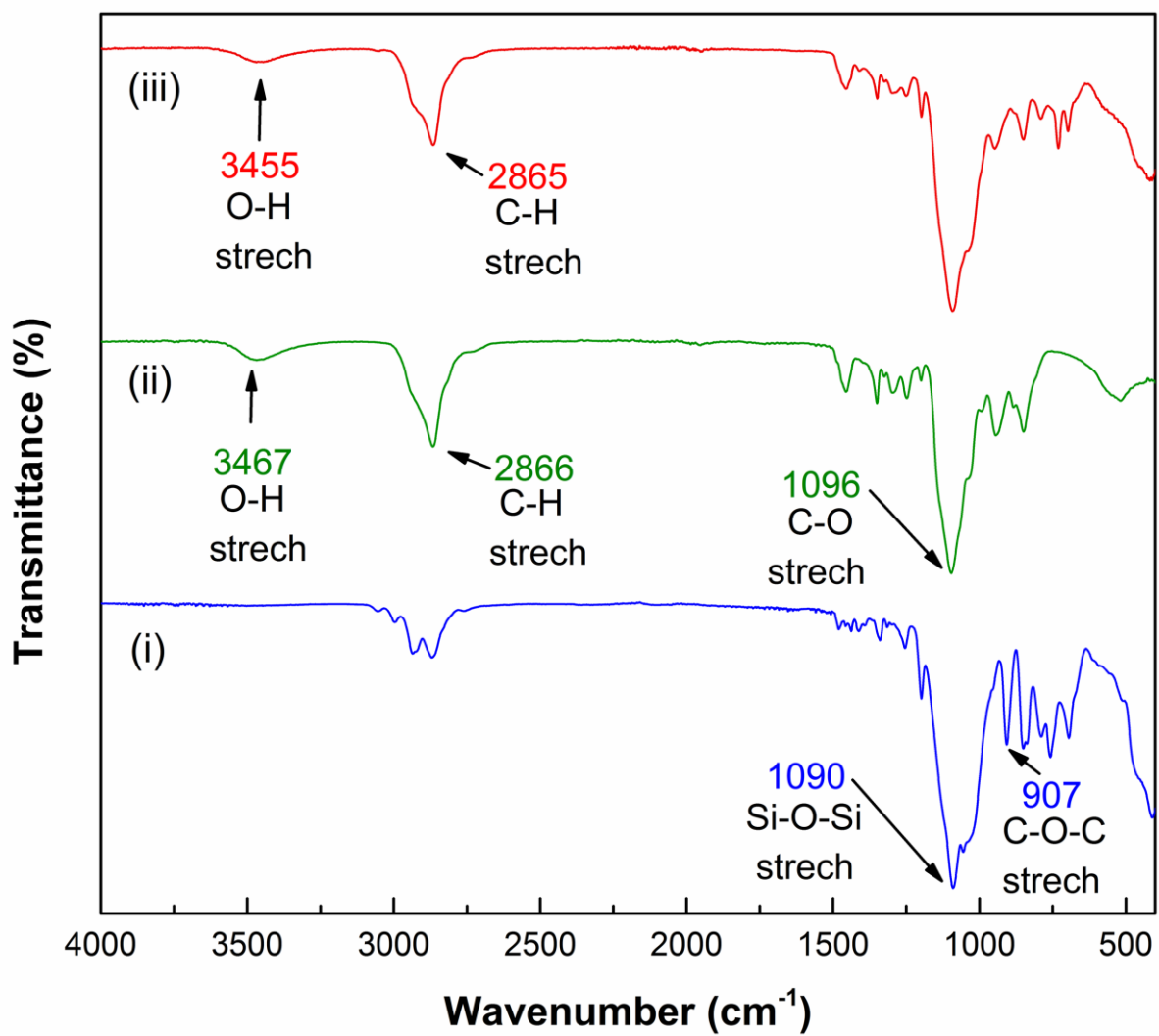


Figure 2

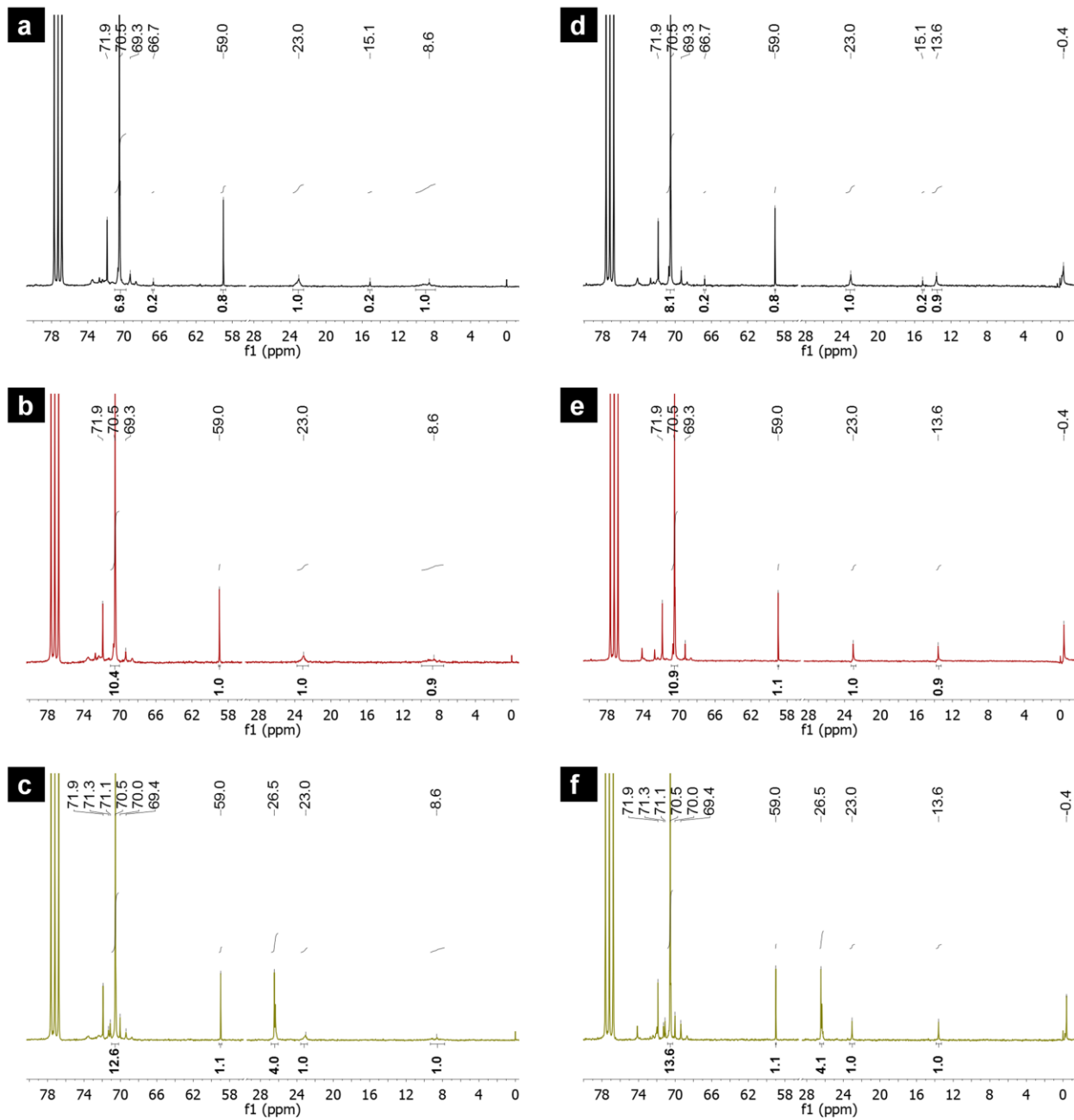


Figure 3

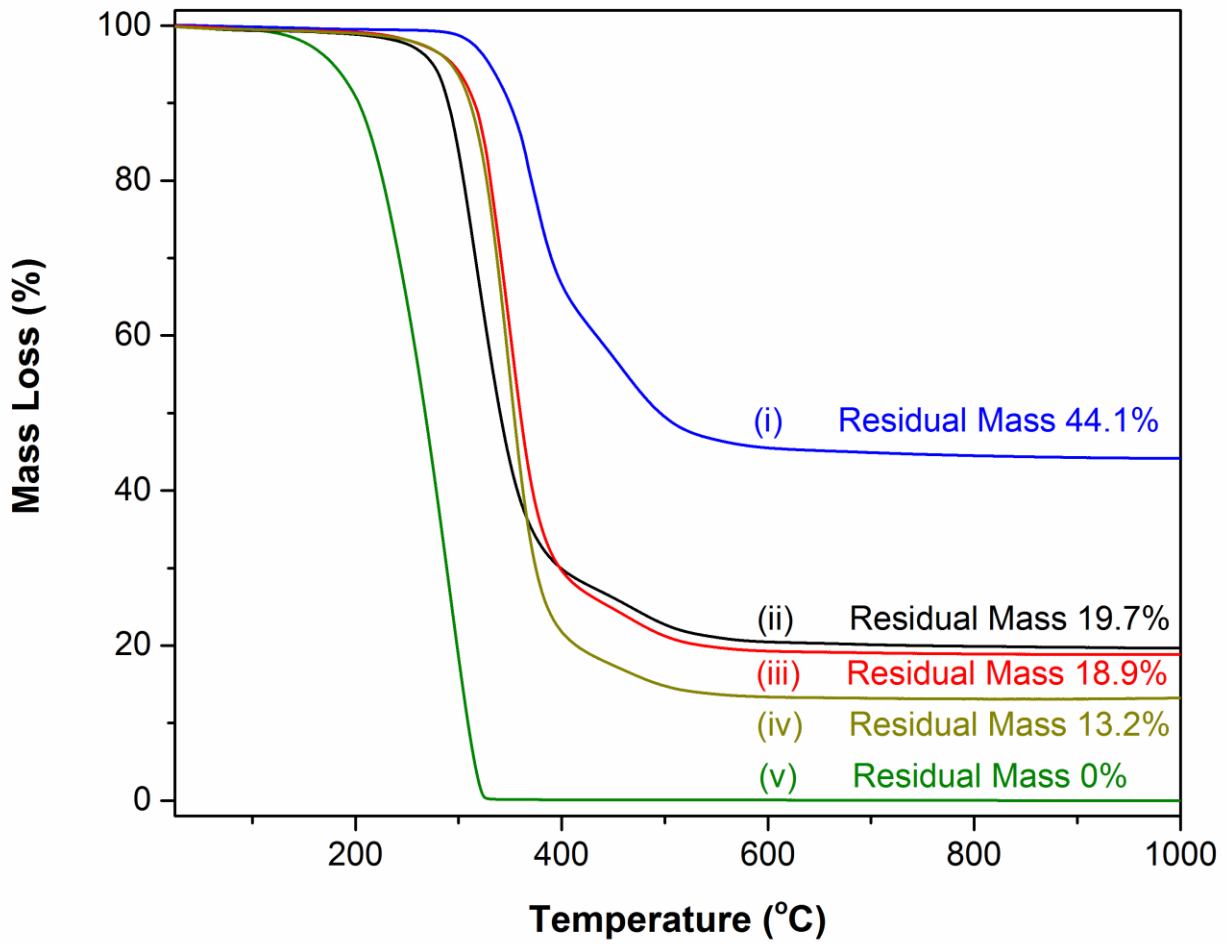


Figure 4

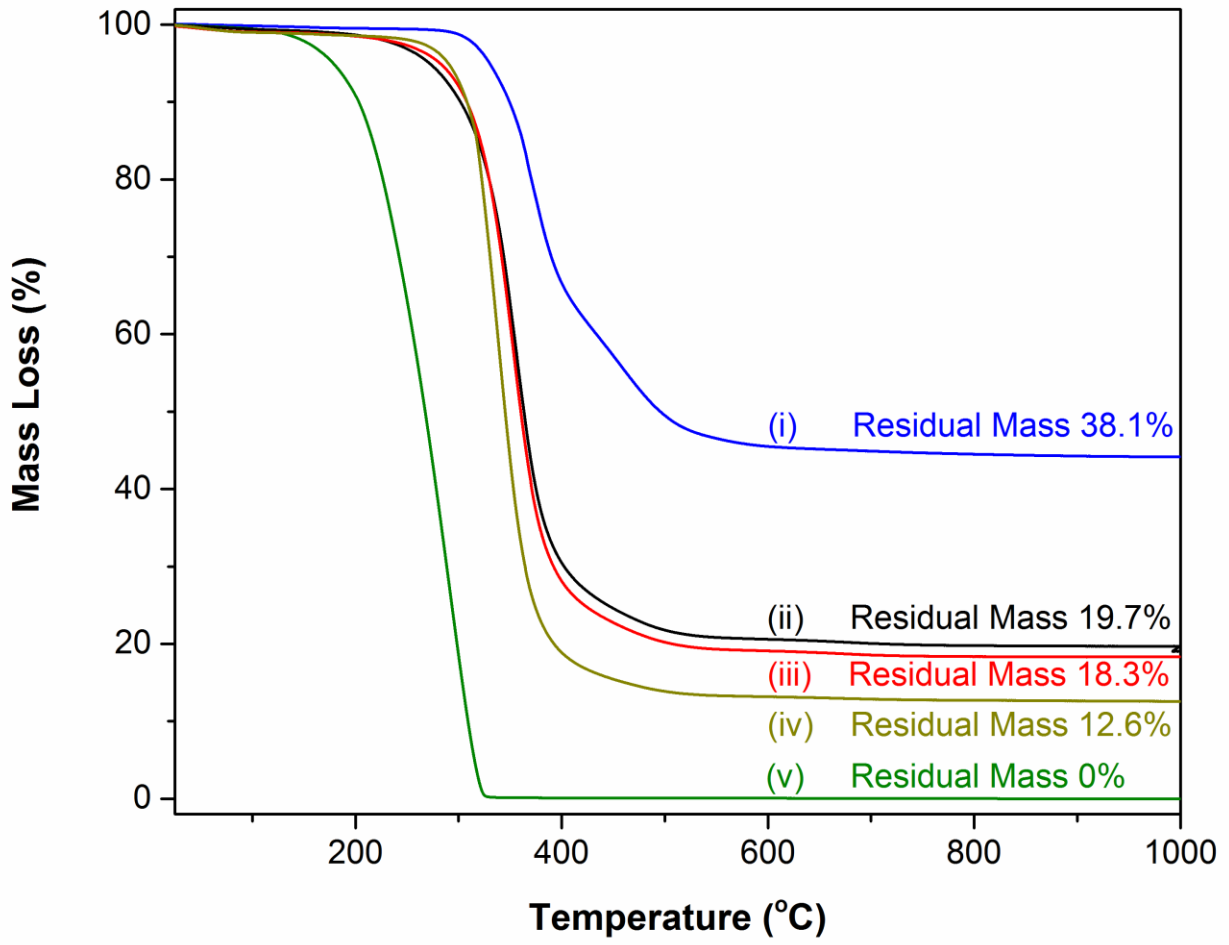


Figure 5

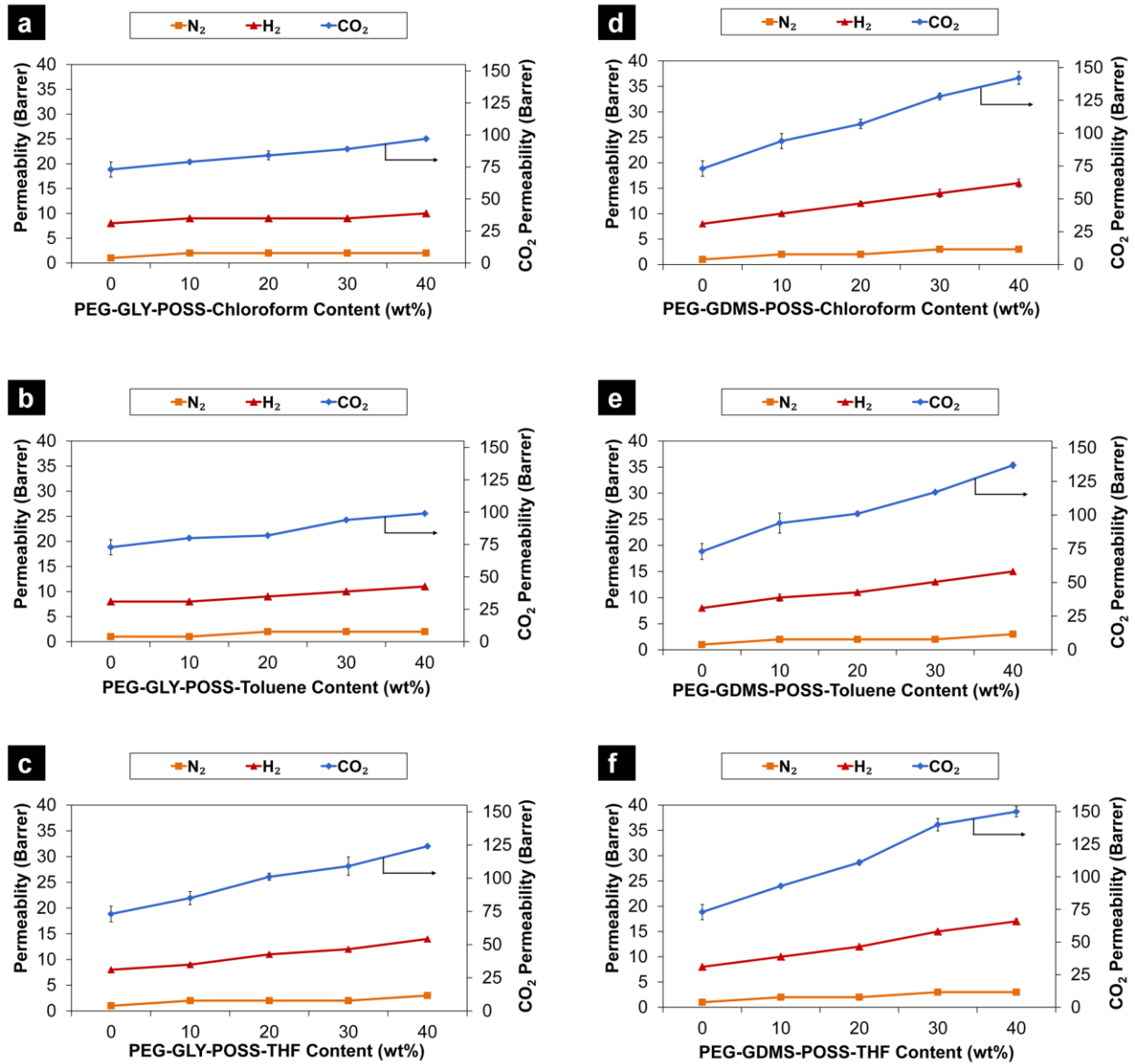


Figure 6

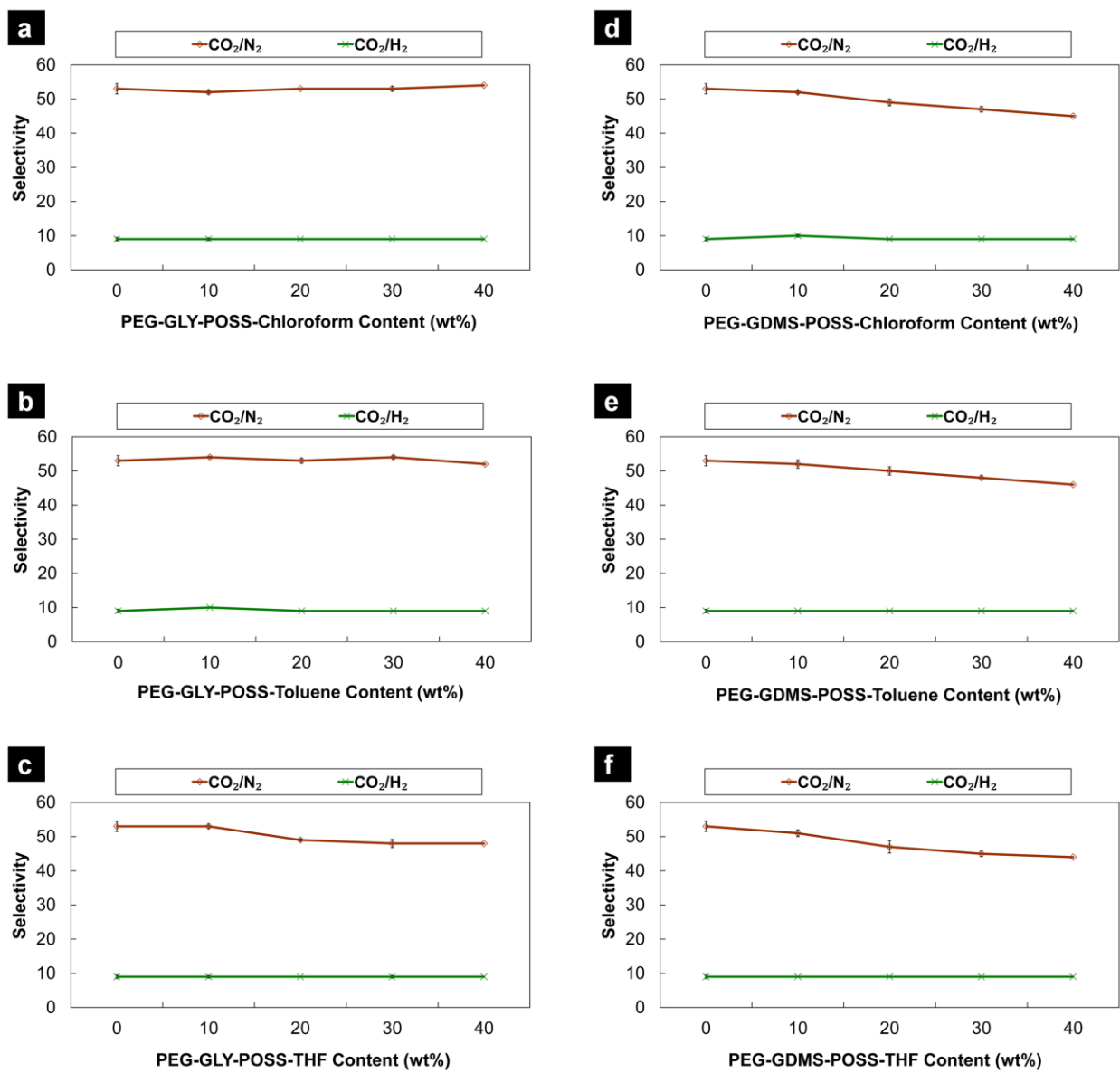
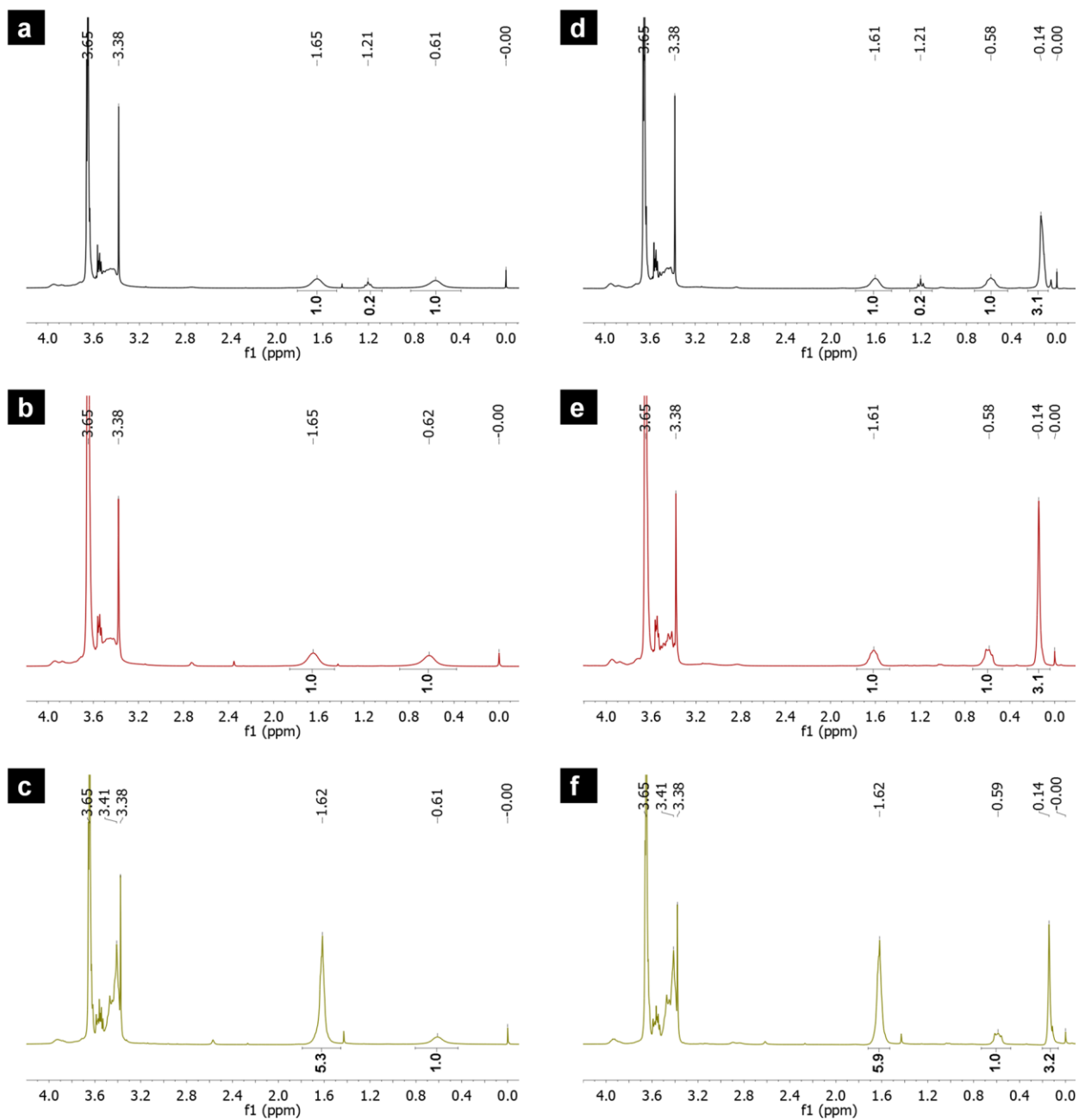


Figure 7

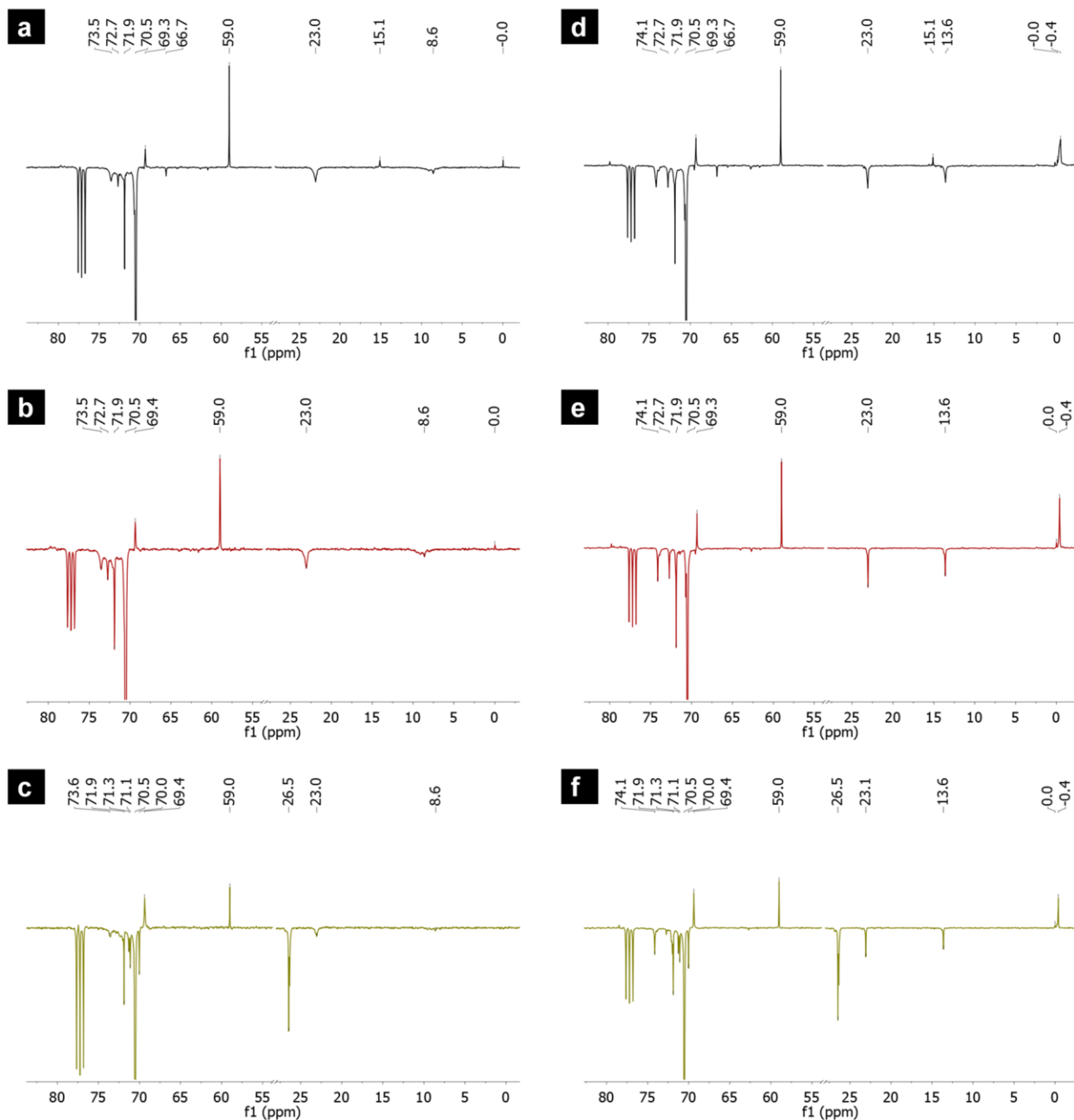
Table 1.

Reactant	Solvent	Acronym of product
Glycidyl POSS and PEG	Chloroform	PEG-GLY-POSS-Chloroform
Glycidyl dimethylsilyl POSS and PEG	Chloroform	PEG-GDMS-POSS-Chloroform
Glycidyl POSS and PEG	Toluene	PEG-GLY-POSS-Toluene
Glycidyl dimethylsilyl POSS and PEG	Toluene	PEG-GDMS-POSS-Toluene
Glycidyl POSS and PEG	THF	PEG-GLY-POSS-THF
Glycidyl dimethylsilyl POSS and PEG	THF	PEG-GDMS-POSS-THF

Electronic Supplementary Information



S 1: ^1H NMR spectra of – (a) PEG-GLY-POSS-Chloroform (b) PEG-GLY-POSS-Toluene (c) PEG-GLY-POSS-THF (d) PEG-GDMS-POSS-Chloroform (e) PEG-GDMS-POSS-Toluene (f) PEG-GDMS-POSS-THF.



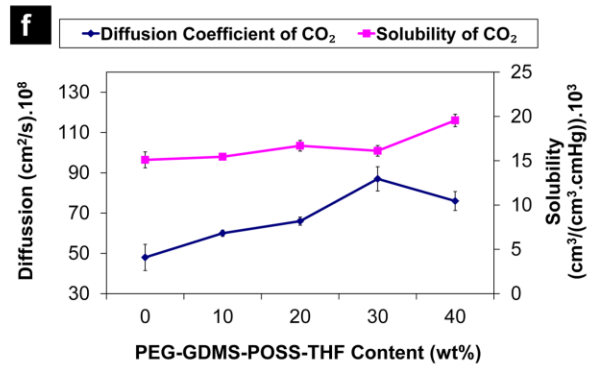
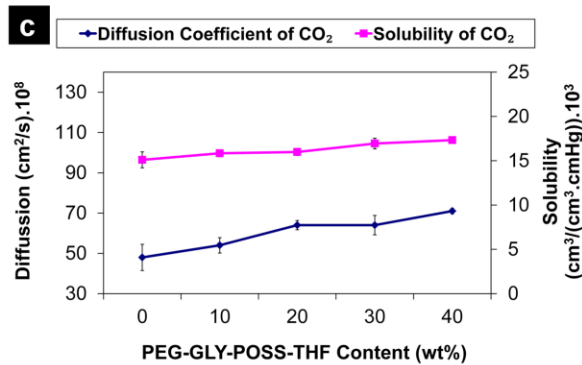
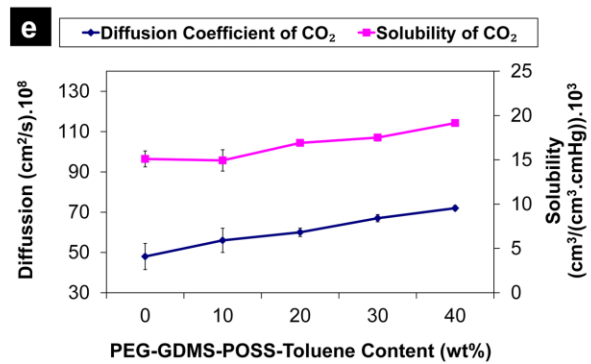
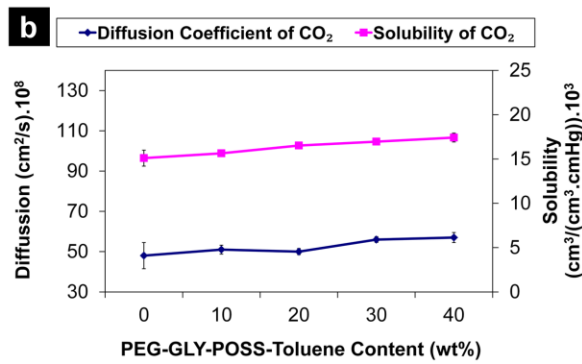
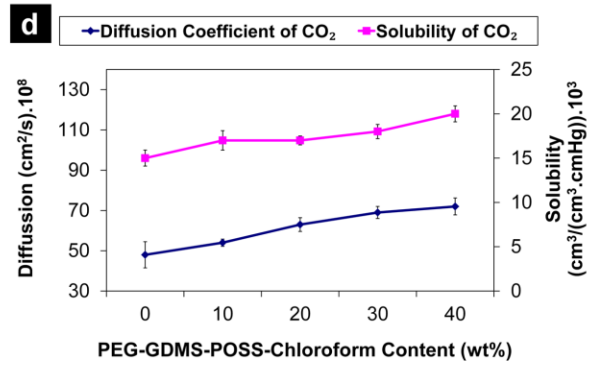
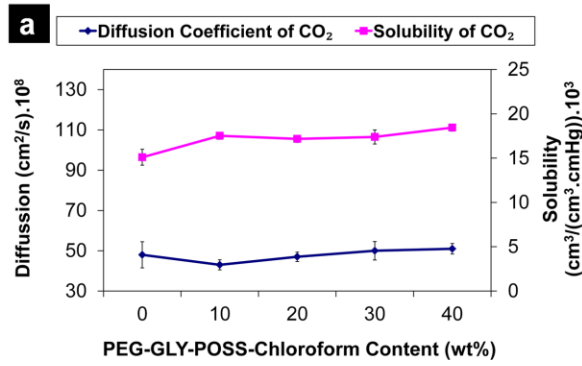
S 2: ^{13}C deptq135 NMR spectra of – (a) PEG-GLY-POSS-Chloroform (b) PEG-GLY-POSS-Toluene (c) PEG-GLY-POSS-THF (d) PEG-GDMS-POSS-Chloroform (e) PEG-GDMS-POSS-Toluene (f) PEG-GDMS-POSS-THF.

S 3: Composition of functionalized POSS nanoparticles after modification with PEG.

Name of POSS	POSS cage content	Total ligand content	Dimethylsilyl spacer content	PEG content (wt%)	THF complex content	Diethyletharate content (wt%)	Rest of the ligand

	(wt%)	(wt%)	(wt%)		(wt%)		content (wt%)
PEG-GLY-POSS- Chloroform	12	88	-	61	-	3	24
PEG-GDMS-POSS- Chloroform	10	90	14	52	-	3	21
PEG-GLY-POSS-Toluene	10	90	-	68	-	-	22
PEG-GDMS-POSS- Toluene	9	91	12	59	-	-	20
PEG-GLY-POSS-THF	8	92	-	53	22	-	17
PEG-GDMS-POSS-THF	7	93	10	48	20	-	15

Note- Glycidyl groups are attached to the POSS cage and dimethylsilyl spacer of Glycidyl POSS® and Glycidyl dimethylsilyl POSS® respectively. Weight percentage of this part after modification with PEG is denoted as “Rest of the ligand content”.



S 4: Diffusion and Solubility of CO₂ as a function of- a) PEG-GLY-POSS-Chloroform content b) PEG-GLY-POSS-Toluene content c) PEG-GLY-POSS-THF content d) PEG-GDMS-POSS-Chloroform content e) PEG-GDMS-POSS-Toluene content f) PEG-GDMS-POSS-THF content. Diffusion of CO₂ is plotted on left Y axis and Solubility of CO₂ right Y axis.